Journal of Materials Chemistry A

PAPER

View Article Online
View Journal | View Issue

Stable ZnO@TiO_2 core/shell nanorod arrays with exposed high energy facets for self-cleaning coatings with anti-reflective properties†

Cite this: *J. Mater. Chem. A*, 2014, **2**, 7313

Ruosong Wang,[ab] Huaqiao Tan,[a] Zhao Zhao,[ac] Guoqiang Zhang,[ac] Laiwen Song,[ac] Wenfei Dong*[b] and Zaicheng Sun*[a]

Received 25th January 2014
Accepted 21st February 2014

DOI: 10.1039/c4ta00455h

www.rsc.org/MaterialsA

Nanostructured metal oxides such as ZnO and TiO_2 have been extensively employed as self-cleaning coatings due to their large band gaps as well as their hydrophilic and photocatalytic properties. We have developed a simple hydrothermal method to coat thin TiO_2 nanosheets with exposed (001) facets onto a ZnO nanorod array. The chemical stability of the ZnO nanorods was great improved due to the existence of the TiO_2 layer. Owing to the porous structure of the ZnO@TiO_2 nanorod arrays, this thin coating layer possesses anti-reflective properties. A transmittance improvement of ~5% was observed for one-side coated FTO glass. This coating also exhibits good hydrophilic properties, after addition of the TiO_2 nanosheets. More importantly, these ZnO@TiO_2 nanorod arrays display excellent photocatalytic properties for the degradation of dye molecules, due to the heterojunction between the ZnO nanorods and TiO_2 nanosheets. This heterojunction facilitates the charge separation of photo generated carriers. Based on the above features, the ZnO@TiO_2 core/shell nanorod array film has many advantages as a self-cleaning coating.

Introduction

Anatase TiO_2 is one of the most promising wide band gap semiconductor materials and has become a topic of intensive study due to its important applications in many fields, such as photocatalysis, dye-sensitized solar cells, photochromic devices and gas sensors.[1–3] The photocatalytic properties of anatase TiO_2 crystals have heavily relied on having access to high-energy facets. Thus, the controlled synthesis of anatase TiO_2 with both exposed high-energy facets and a high surface area is, technologically speaking, very important. Since 2008, when Lu *et al.* successfully prepared anatase TiO_2 crystals with a high percentage of exposed (001) facets,[4] various TiO_2 nanostructures with a high number of reactive facets have been developed.[5–8] The photocatalytic performance is significantly improved when TiO_2 nanostructures possess this well-defined crystal facet. This provides a great opportunity for the fabrication high performance self-cleaning coatings.

Self-cleaning coatings have attracted extensive attention in recent research and also commercial applications, such as building glass, eyeglasses, and solar cell modules. Generally, self-cleaning coatings can be classified into two types, hydrophobic and hydrophilic. On a hydrophilic coating, water is made to spread out (water sheeting) over the surface, which carries away dirt and other impurities, whereas using the hydrophobic technique, water droplets slide and roll over the surface, thereby cleaning them.[9] TiO_2 is an effective self-cleaning material due to its excellent stability, good photocatalytic performance and hydrophilic properties. However, the coatings developed thus far have always enhanced the surface reflection of the transparent substrates due to the large refractive index of TiO_2 ($n = 2.52$ for anatase; 2.76 for rutile). Reflection at the air–glass interface is about 4% for normal incident light, whereas at the air–TiO_2 interface the reflection of normal incident light can be as high as 20%, as described using the simplified version of Fresnel's equation. For many practical applications, for example, solar cells and eyeglasses, self-cleaning coatings with low surface reflection and high transmission are highly desirable.

Anti-reflection (AR) coatings are widely used to reduce the surface reflection of optical devices. The principle behind AR is interference of the reflected light from the air–coating and coating–substrate interfaces. Thus, an AR coating should exhibit a refractive index between that of the air and the substrate. An ideal homogeneous single-layer AR coating should satisfy the following condition: $n_c = (n_a \times n_s)^{0.5}$, where

[a]*State Key Laboratory of Luminescence and Applications, Changchun Institute of Optics, Fine Mechanics and Physics, Chinese Academy of Science, 3888 East Nanhu Road, Changchun 130033, People's Republic of China. E-mail: sunzc@ciomp.ac.cn*

[b]*Suzhou Institute of Biomedical Engineering and Technology, Chinese Academy of Science, 88 Keling Road, Suzhou 215163, People's Republic of China. E-mail: wenfeidong@126.com*

[c]*University of Chinese Academy of Sciences, Beijing, P.R. China*

† Electronic supplementary information (ESI) available: EDAX, XRD and degradation curve of FTO glass. See DOI: 10.1039/c4ta00455h

n_c, n_a, and n_s are the refractive indices of the coating, air and substrate, respectively.[10] Since this value is lower than that of any homogeneous dielectric material, AR coatings always adopt 2- or 3-dimensional porous structures to meet the requirements for a very low average refractive index.[11–13] ZnO nanorod,[14,15] Si nanodome[16] and Si nanocone[17] array coatings have all been employed as AR coatings. However, the chemical stability of ZnO has impeded its further application as an AR coating.

ZnO nanorod arrays possesses a unique one dimensional nanostructure and a single crystalline phase within each nanorod, which are beneficial for improving charge transportation and the photocatalytic activity.[18–21] However, ZnO is a chemically unstable material that can be dissolved in both acidic and basic solutions.[22] To improve the stability of the ZnO nanorod arrays, a few groups have reported the preparation of ZnO@TiO_2 core/shell nanowires *via* an extra sol–gel route or physical deposition methods for use in dye sensitized solar cells, UV detectors and as photocatalysts.[23–26] In addition, ZnO nanorod arrays provide relatively lower surface areas compared with mesoporous structures. According to the report of Lou *et al.*,[8,27] TiO_2 spheres composed of nanosheet structures with exposed highly reactive (001) facets can be prepared *via* a simple hydrothermal route. In this work, we successfully synthesized ZnO nanorod arrays coated with a layer of TiO_2 nanosheets to form ZnO@TiO_2 nanorod arrays *via* a modified version of Lou's route. After calcination, a layer of TiO_2 nanosheets with highly reactive (001) facets was formed on the highly crystalline ZnO nanorod surface. This TiO_2 shell layer not only improves the chemical stability of the coating, but also imparts improved hydrophilicity and photocatalytic activity upon the ZnO@TiO_2 coating layer. In addition, the ZnO@TiO_2 nanorod array structure results in an excellent anti-reflective effect, which affords better transmittance. This ZnO@TiO_2 nanorod array could be employed as a highly transparent self-cleaning coating for LEDs or photovoltaic devices.

Experimental

Chemicals and materials

Zinc acetate dehydrate ($Zn(CH_3COO)_2 \cdot 2H_2O$, AR grade) was purchased from the Shantou Xilong Chemical factory, ethanolamine (AR grade) from the Sinopharm Chemical Reagent Co. Ltd., and zinc nitrate hexahydrate ($Zn(NO_3)_2 \cdot 6H_2O$, 99% by weight) from the Tianjin Guangfu Chemical Reagent Co. Ltd. All other reagents, *e.g.*, 2-methoxyethanol (AR grade), hexamethylenetetramine (HMTA, 99.5% by weight), diethylenetriamine (DETA, 99% by weight), titanium(IV) isopropoxide (98% by weight) and rhodamine B (RhB, AR grade), are all purchased from the Aladdin Reagent Company. All of the materials in these experiments were used without further purification.

Synthesis of the ZnO nanorod arrays

The ZnO nanorod arrays were synthesized *via* a modified version of Yang's route.[23–26] In a typical reaction, zinc acetate dihydrate and ethanolamine were mixed in a 1 : 1.2 molar ratio in 25 mL 2-methoxyethanol to ensure the concentration of $Zn(CH_3COO)_2$ was 0.2 mol L^{-1}. The above solution was stirred at 60 °C for 30 min, and then spin-coated (3000 rpm for 1 min) onto FTO glass substrates, which were ultrasonically cleaned, in order, with deionized water, ethanol and acetone. Next, we placed the pretreated FTO glass substrates in an electric oven at 400 °C for 2 h to obtain ZnO grains. Furthermore, zinc nitrate hexahydrate and HMTA were dissoved in 100 mL deionized water to give a concentration of $Zn(NO_3)_2$ of 25 mmol L^{-1} and a 1 : 1 molar ratio of $Zn(NO_3)_2$: HMTA. The ZnO nanorod arrays were grown on the FTO substrates from the ZnO grains by soaking in the above solution at 70 °C for 4 h.

Synthesis of the ZnO@TiO_2 core/shell nanorod array films

The ZnO nanorod film was placed into a Teflon lined stainless steel autoclave, which contained 7.5 μL DETA, 10.5 mL isopropyl alcohol (AR grade, Beijing Chemical Works) and a variable amount of titanium(IV) isopropoxide. The sealed autoclave was heated to 180 °C for 12 h in an electric oven. Following this, the reaction autoclave was naturally cooled to room temperature. The as-prepared samples were gently rinsed with ethanol and acetone and dried at room temperature. Finally, the samples were annealed at 400 °C for 2 h to form the crystal phase of TiO_2.

Chemical stability tests

The as-obtained ZnO and ZnO@TiO_2 nanorod arrays were immersed into pH = 0–14 aqueous solutions for 30 minutes. The samples were then rinsed with distilled water, ethanol and acetone. The optical transmission was monitored with a Shimadzu UV-3600 UV-Vis spectrophotometer.

Rhodamine B (RhB) photodegradation activity measurements

A 5000 ppm RhB ethanol solution was used as a stock solution in our experiments. Four selected samples were employed for comparison, *i. e.*, a bare FTO glass substrate (marked as FTO), a ZnO nanorod array (marked as ZnO), and two ZnO@TiO_2 core/shell nanorod arrays prepared using either 30 μL or 15 μL titanium(IV) isopropoxide as mentioned in the experimental section (marked as TiO_2-30 and TiO_2-15, respectively). All of these samples were immersed in a RhB ethanol solution in the dark for 24 h. The samples were then taken out for to dry naturally in order to form a layer of RhB on the sample surface. The photocatalytic activity of the samples was evaluated through the decolorization of rhodamine B (RhB) under a 300 W high voltage UV light xenon lamp (with a central wavelength of 360 nm) at a distance of 15 cm. The samples were not subjected to any previous treatment before irradiation and were covered from any other source of light during the measurements to ensure that a adsorption–desorption equilibrium between the TiO_2 catalyst and RhB was reached. After irradiation for the designated time, the RhB concentration was monitored using the absorbance value at the maximum peak (553 nm) with a Shimadzu UV-3600 UV-Vis spectrophotometer.

Characterization

Structural and elemental chemical composition analyses of the samples were carried out using field emission scanning electron microscopy (FESEM) and energy-dispersive X-ray spectroscopy (EDX), which were measured with a JEOL JSM 4800F microscope. Crystallographic analyses were carried out using transmission electron microscopy (TEM) with a FEI Tecnai G2 microscope operated at 200 kV. The UV-Vis-NIR transmittance spectra were recorded on a Shimadzu UV-3600 UV-Vis-NIR scanning spectrophotometer. The contact angle (CA) measurements were carried out by dropping deionized water onto the substrates at room temperature using a CA system (KRUSS GH-100 universal surface tester). The wettability of the samples was characterized with a CCD camera interfaced with an optical microscope, which was arranged in a goniometric setup.

Results and discussion

As shown in the schematic diagram in Fig. 1, the ZnO nanorods were grown from the ZnO seed layer on the FTO through a hydrothermal route as in the previous reports.[18] Recently, Lou *et al.* developed a simple hydrothermal route to synthesize TiO_2 spheres composed of nanosheets with exposed highly reactive (001) facets, which possessed high surface area and good photocatalytic activity.[8] We combined the TiO_2 nanosheet structures and highly crystalline ZnO nanorod arrays together and obtained ZnO@TiO_2 core/shell nanorod arrays *via* a modified version of Lou's route. This structure possesses a large surface area, highly reactive (001) facets, and highly crystalline ZnO nanorods for electron transportation. These merits will boost the photocatalytic performance of the ZnO@TiO_2 coating.

Fig. 2 shows planar and cross-sectional SEM images of ZnO and ZnO@TiO_2 core/shell nanorod array thin films on FTO glass. Fig. 2A shows that ZnO nanorods with defined facet structures are normal on the substrate. In order to obtain high transparency, the thickness of the ZnO nanorod thin films was controlled to about 300–400 nm by tuning the reaction

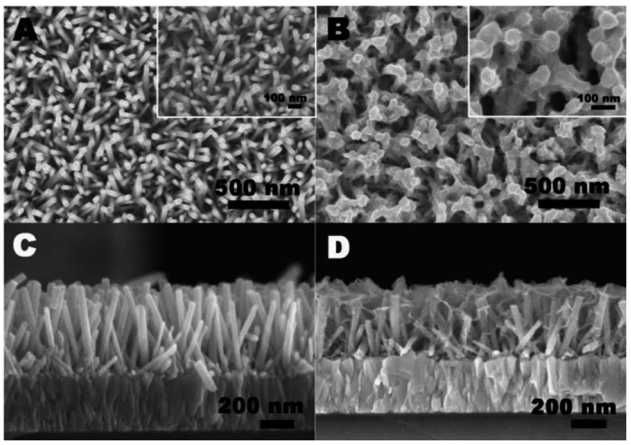

Fig. 2 Field emission scanning electron microscopy (FESEM) of the ZnO nanorod array and the ZnO@TiO_2 core/shell nanorod array. (A) A planar view of the ZnO nanorod array film. Inset: a high magnification image. (B) A planar view of the TiO_2-30 sample. Inset: a high magnification image. (C) and (D) are the corresponding cross sectional views of (A) and (B), respectively.

conditions (Fig. 2C). The TiO_2 nanosheets were grown on the ZnO nanorod surfaces *via* the modified version of Lou's route.[8] The planar view image in Fig. 2B shows that the ZnO nanorod surface becomes rough and rounded compared with the original ZnO nanorods. The cross-sectional image of the ZnO@TiO_2 nanorod array in Fig. 2C shows that some petal-like TiO_2 shells have formed and connected between the ZnO nanorods. The chemical composition of the product was confirmed by EDX analysis (Fig. S1†), which showed strong Zn, Ti and O signals, indicating that Zn, Ti, and O elements coexist in the sample. However, both the anatase and rutile TiO_2 crystalline phase were barely observed with mainly ZnO and SnO_2 peaks in the XRD measurements (Fig. S2†). The broad band around 25° is a result of the amorphous silicate glass substrate. There is a relatively weak peak at 25° in the XRD pattern of TiO_2-30, which

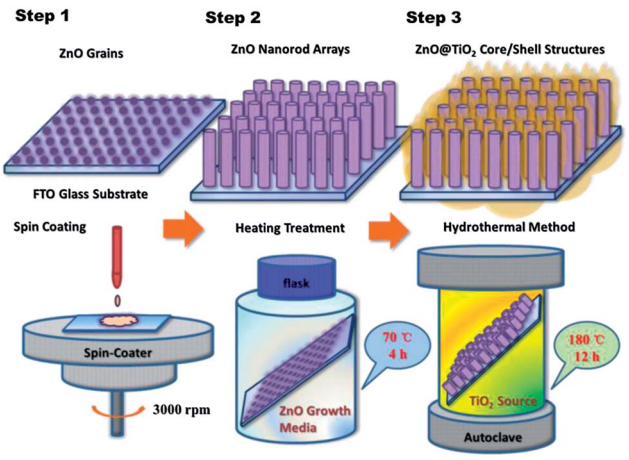

Fig. 1 Schematic diagram of the preparation procedure for the ZnO@TiO_2 core/shell nanorod array films based on an FTO glass substrate using a hydrothermal method.

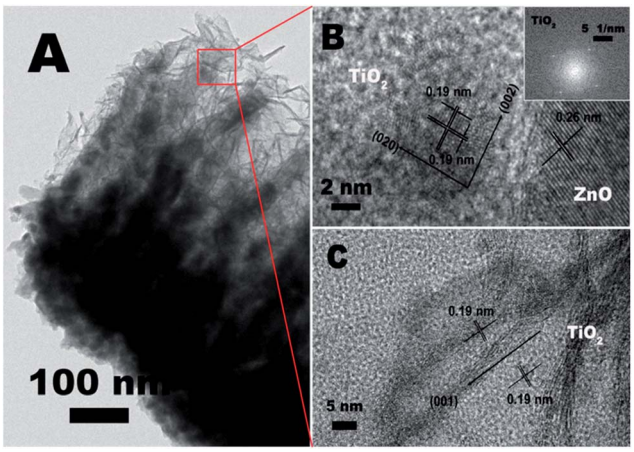

Fig. 3 (A) Transmission electron microscopy (TEM) images of the ZnO@TiO_2 nanorod arrays. (B and C) High resolution TEM images of the red square shown in A. The inset in B shows the FFT pattern indexed to the [001] zone.

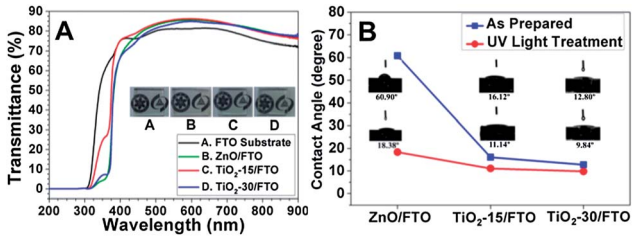

Fig. 4 (A) The transparency of the FTO substrate and thin films of ZnO nanorod arrays coated with different thicknesses of TiO_2 nanosheets. The insets show the corresponding optical pictures. (B) The contact angle of the ZnO nanorod array thin films coated with different thicknesses of TiO_2 nanosheets. The insets show the contact angle optical images.

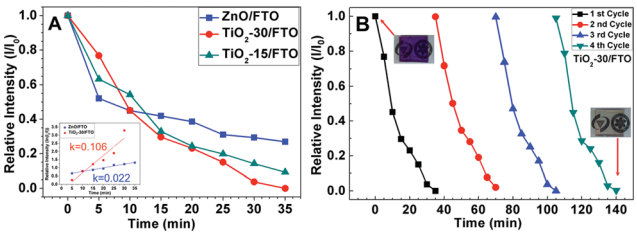

Fig. 5 (A) Comparison of the photocatalytic degradation rates of rhodamine B (RhB) of the selected samples. Inset: *ln*-plot of the degradation rates of the ZnO nanorod array film and the TiO_2-30 sample. (B) Cycling degradation curves of the TiO_2-30 sample with optical pictures of the initial and final state in the cycle.

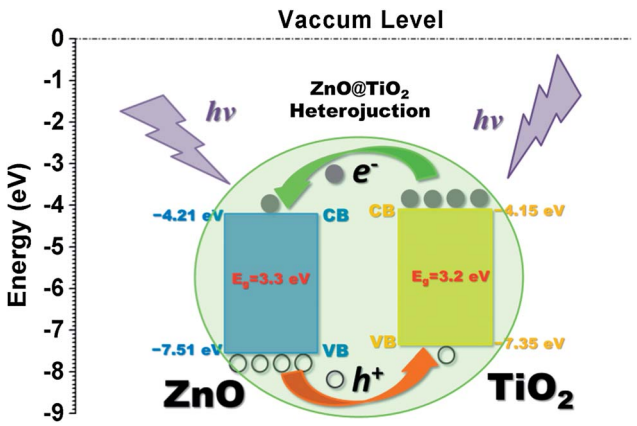

Fig. 6 An energy level scheme of ZnO and TiO_2. The heterojunction formed between ZnO and TiO_2 promotes charge separation.

may be associated with anatase TiO_2. The probable reason for this is that the TiO_2 layer is too thin to obtain a strong XRD signal in our case. We did observe a strong XRD signal for TiO_2 when the ZnO nanorods were coated with a thicker TiO_2 layer prepared at a higher concentration of Ti precursor (Fig. S2†).

The crystalline phase of TiO_2 was confirmed through transmission electron microscopy (TEM) images. Fig. 3 shows that the ZnO nanorods were fully covered by the TiO_2 nanosheets. There are thin petal-like nanosheets between the ZnO nanorods. High resolution TEM images (HRTEM, Fig. 3B and C) indicate that the petal-like structures have clear crystalline lattice structures. It can be observed that there are two sets of lattices, which are oriented perpendicular to each other with an equal interfringe spacing of 0.19 nm, corresponding to the anatase (020) and (200) planes. The fast Fourier transform (FFT) pattern of the same region (Fig. 3B, inset) can be indexed to diffraction spots of the [001] zone.[4] According to Lou's report, the TiO_2 nanosheets are bound by (001) facets on both of the exposed sides.[8] Fig. 3C displays a HRTEM image taken of the interspace between the ZnO nanorods. The dark outline in the TEM image (Fig. 3A) demarcates the edge of the curved nanosheets oriented approximately vertical to the supporting film. This dark line can be used to estimate the thickness of the nanosheets as only ~3 nm, which is close to the Lou's report.[8]

For self-cleaning coatings on glass, transparency is an important factor. Fig. 4A shows the transmittance of the bare FTO substrate, after coating with the ZnO nanorod array, and the ZnO@TiO_2 nanorod array thin film. The bare FTO glass shows ~80% transmittance in the whole visible light region. After coating with the ZnO nanorod array thin film, the transmittance of the FTO glass was improved from 80% to 86%. This improvement is not only at a single wavelength point, but ~5% of increase across the whole spectrum (400–900 nm) due to the unique nanorod array structure, which lowerd the refractive index of the coating layer. In addition, for the FTO glass coated with the ZnO nanorod array, UV light (λ < 380 nm) was effectively cut off, due to the large band gap of ZnO (3.37 eV). This UV cut function will be beneficial to potential applications in solar cells and LED devices. After growing TiO_2 nanosheets onto the ZnO nanorods, the transparency of substrate still remains at ~85%, as before the coating. However, too thick an TiO_2 layer may result in a small loss in transmittance because the TiO_2 nanosheets fill in the space between the ZnO nanorods, results in an increase of the refractive index of the coating layer. Furthermore, the stabilities of the ZnO nanorod film and the TiO_2-30 samples were measured in different pH solutions (Fig. S3†). When the pH value is below 4 and above 10, the transmittance of the ZnO nanorod film drops dramatically to below that of the bare FTO glass substrate (even less than 80%), owing to corrosion of the ZnO nanorod film by acidic or basic solutions. However, the transmittance of the TiO_2-30 sample only slightly fluctuated and remained above 83%, indicating that the TiO_2 nanosheets effectively prevent the ZnO nanorods from corroding due to the surrounding medium. The stability of the ZnO nanorods was dramatically improved by the TiO_2 outer layer.

For hydrophilic self-cleaning coatings, the wettability is another important factor. Although the oxide surface is hydrophilic, the nanorod array, in general, is hydrophobic owing to the existence of air pockets.[28] The contact angle can be employed to characterize the wettability of the coating layer (Fig. 4B). The FTO glass with the ZnO nanorod array thin film exhibits a contact angle of about 61°. After UV illumination for 5 min, the ZnO nanorod array thin film shows hydrophilic properties and the contact angle decreases to 18°. When the TiO_2 nanosheets were coated onto the ZnO nanorod array, the contact angle decreased to 16°. A thicker TiO_2 nanosheet coating results in a smaller contact angle (12°). After UV light

illumination, the contact angle can be further decreased to lower than 10°.

A key issue for hydrophilic self-cleaning coatings is the photocatalytic activity of the coating layer. In this report, rhodamine B (RhB) was chosen as a model dye molecule to demonstrate the photocatalytic activity of the ZnO@TiO_2 nanorod array thin films. It is hard to coat a thick RhB layer onto bare FTO glass. Fig. S4† shows the degradation of RhB on FTO glass. It clearly shows self-degradation during the first 5 minutes. The degradation curve then tends to flatten, indicating that the degradation rate is very slow. Self-degradation makes up a large percentage of the degradation for the very thin RhB layer on the FTO substrate. For the ZnO nanorod array on the FTO sample, the degradation curve also shows a rapid decrease within the first 5 minutes, indicating that self-degradation may happen within this period (Fig. 5A). After 5 minutes, the degradation rate stays at a constant rate ($k = 0.022$ min^{-1}) as shown in the inset of Fig. 5A. After 35 minutes illumination under UV-Vis light, only ~60% RhB was degraded by the ZnO nanorod array. When the ZnO nanorod array was coated with TiO_2 nanosheets, the RhB was absorbed onto the TiO_2 nanosheet surface. The degradation curve shows a smooth decrease trend with illumination time. The degradation rate is about 0.106 min^{-1}, which is ~5 times better than the ZnO nanorod array thin film. After 35 minutes illumination under UV-Vis light, about 98% RhB was degraded by the ZnO@TiO_2 nanorod array. The substrate turned from dark purple to transparent under the light illumination. With the TiO_2 nanosheet layer, the photocatalytic capability is significantly enhanced because the TiO_2 nanosheets improved the surface area of the ZnO nanorod array. In addition, the conduction bands of anatase TiO_2 and ZnO are −4.15 and −4.21 eV, respectively. Due to the type II heterojunction formed between ZnO and TiO_2, the photo-generated electrons of TiO_2 can inject into the conduction band of ZnO. The photo-generated holes of ZnO can also be easily transferred into the valance band of TiO_2. This promotes charge separation (Fig. 6). Fig. 5B shows the durability of the ZnO@TiO_2 nanorod array for the photocatalytic degradation of RhB under UV-Vis irradiation. After each recycled experiment, the photocatalytic activity remains unchanged.

Conclusions

We have developed a ZnO@TiO_2 nanorod array thin film coating on an FTO substrate *via* a hydrothermal route. The coating exhibits good transparency and hydrophilic properties. The ZnO@TiO_2 nanorod array displays very good photocatalytic activity for the degradation of dye molecules and good durability because of the heterojunction between the ZnO nanorods and the TiO_2 layer, which is composed of TiO_2 nanosheets with exposed (001) facets. The heterojunction facilitates the charge separation of photo generated carriers.

Acknowledgements

The authors thank Prof. Junqi Sun for their great help in the contact angle measurements. Financial support from the National Natural Science Foundation of China (no. 61306081, 21301166, 21201159, 61176016, 91123029), International S&T Cooperation Program of China (no. 2013DFR70490), Science and Technology Department of Jilin Province (no. 20130522142JH, 20130522127JH, 20121801) is gratefully acknowledged. ZS thanks the support of the "Hundred Talent Program" of CAS, and the Innovation and Entrepreneurship Program of Jilin.

Notes and references

1 X. Chen and S. S. Mao, *Chem. Rev.*, 2007, **107**, 2891–2959.
2 M. Graetzel, R. A. J. Janssen, D. B. Mitzi and E. H. Sargent, *Nature*, 2012, **488**, 304–312.
3 M. A. Henderson, *Surf. Sci. Rep.*, 2011, **66**, 185–297.
4 H. G. Yang, C. H. Sun, S. Z. Qiao, J. Zou, G. Liu, S. C. Smith, H. M. Cheng and G. Q. Lu, *Nature*, 2008, **453**, 638–641.
5 J. Pan, G. Liu, G. Q. Lu and H.-M. Cheng, *Angew. Chem., Int. Ed.*, 2011, **50**, 2133–2137.
6 C. Z. Wen, H. B. Jiang, S. Z. Qiao, H. G. Yang and G. Q. Lu, *J. Mater. Chem.*, 2011, **21**, 7052.
7 Z. Zhao, Z. Sun, H. Zhao, M. Zheng, P. Du, J. Zhao and H. Fan, *J. Mater. Chem.*, 2012, **22**, 21965.
8 J. S. Chen, Y. L. Tan, C. M. Li, Y. L. Cheah, D. Luan, S. Madhavi, F. Y. C. Boey, L. A. Archer and X. W. Lou, *J. Am. Chem. Soc.*, 2010, **132**, 6124–6130.
9 V. A. Ganesh, H. K. Raut, A. S. Nair and S. Ramakrishna, *J. Mater. Chem.*, 2011, **21**, 16304.
10 B. E. Yoldas, *Appl. Opt.*, 1980, **19**, 1425–1429.
11 J. A. Hiller, J. D. Mendelsohn and M. F. Rubner, *Nat. Mater.*, 2002, **1**, 59–63.
12 S. Walheim, E. Schäffer, J. Mlynek and U. Steiner, *Science*, 1999, **283**, 520–522.
13 H. Hattori, *Adv. Mater.*, 2001, **13**, 51–54.
14 Y.-C. Chao, C.-Y. Chen, C.-A. Lin, Y.-A. Dai and J.-H. He, *J. Mater. Chem.*, 2010, **20**, 8134–8138.
15 J. Y. Chen and K. W. Sun, *Sol. Energy Mater. Sol. Cells*, 2010, **94**, 930–934.
16 J. Zhu, C. M. Hsu, Z. Yu, S. Fan and Y. Cui, *Nano Lett.*, 2010, **10**, 1979–1984.
17 J. Zhu, Z. Yu, G. F. Burkhard, C. M. Hsu, S. T. Connor, Y. Xu, Q. Wang, M. McGehee, S. Fan and Y. Cui, *Nano Lett.*, 2009, **9**, 279–282.
18 L. E. Greene, M. Law, J. Goldberger, F. Kim, J. C. Johnson, Y. Zhang, R. J. Saykally and P. Yang, *Angew. Chem., Int. Ed.*, 2003, **42**, 3031–3034.
19 T. Zhang, W. Dong, M. Keeter-Brewer, S. Konar, R. N. Njabon and Z. R. Tian, *J. Am. Chem. Soc.*, 2006, **128**, 10960–10968.
20 X. Huang, L. Shang, S. Chen, J. Xia, X. Qi, X. Wang, T. Zhang and X.-M. Meng, *Nanoscale*, 2013, **5**, 3828–3833.
21 L. Wang, Y. Zheng, X. Li, W. Dong, W. Tang, B. Chen, C. Li, X. Li, T. Zhang and W. Xu, *Thin Solid Films*, 2011, **519**, 5673–5678.
22 R. Comparelli, E. Fanizza, M. L. Curri, P. D. Cozzoli, G. Mascolo and A. Agostiano, *Appl. Catal., B*, 2005, **60**, 1–11.
23 S. Panigrahi and D. Basak, *Nanoscale*, 2011, **3**, 2336–2341.

24 X. Yan, C. Zou, X. Gao and W. Gao, *J. Mater. Chem.*, 2012, **22**, 5629–5640.
25 M. Law, L. E. Greene, A. Radenovic, T. Kuykendall, J. Liphardt and P. Yang, *J. Phys. Chem. B*, 2006, **110**, 22652–22663.
26 D. Chen, H. Zhang, S. Hu and J. Li, *J. Phys. Chem. C*, 2007, **112**, 117–122.
27 J. S. Chen, J. Liu, S. Z. Qiao, R. Xu and X. W. Lou, *Chem. Commun.*, 2011, **47**, 10443–10445.
28 X. Feng, F. Lin, M. Jin, J. Zhai, L. Jiang and D. Zhu, *J. Am. Chem. Soc.*, 2003, **126**, 62–63.